Contrib Mineral Petrol (2003) 144: 416–427
DOI 10.1007/s00410-002-0405-2

Alfons Berger · Claudio L. Rosenberg

Preservation of chemical residue-melt equilibria in natural anatexite: the effects of deformation and rapid cooling

Received: 8 April 2002 / Accepted: 31 July 2002 / Published online: 11 September 2002

Abstract A combined petrologic, textural and chemical approach is used to interpret the relationship between chemical exchange and deformation during partial melting of a granodioritic gneiss in the contact aureole of the Bergell Pluton (Central Alps). In contrast to most regional metamorphic anatexites, chemical equilibrium between residue and segregated melt was attained and preserved by several elements, as shown by their present distribution. Equilibrium involved both the major and the trace elements hosted in the rock-forming minerals and the light rare earth elements (LREE), hosted primarily in allanite. Equilibrium with respect to LREEs was achieved because allanite had a reactive behaviour during water-present melting, in contrast to the refractive behaviour of xenotime, which mostly controls the distribution of the HREE's. The attainmenffffft and preservation of equilibrium between leucosome and residue requires peculiar boundary conditions. We propose that the achievement of equilibrium between melt and residue was promoted by deformation, operating via a mechanism of melt present granular flow (i.e. dissolution-accommodated grain-boundary sliding active during partial melting). Microstructural observations indicate that melt-present granular flow was the dominating deformation mechanism in these anatexites. The preservation of residue–melt equilibrium is inferred to result from rapid cooling under contact metamorphic conditions and from the lack of deformation below the solidus.

A. Berger (✉)
Institute for Geological Sciences,
University of Bern, Baltzerstr. 1, Bern, Switzerland
E-mail: berger@geo.unibe.ch
Tel.: +44-31-6318493
Fax: +41-31-6314843

C.L. Rosenberg
Fachbereich Geowissenschaft, Freie Universität Berlin,
Malteser Str. 74-100, Berlin, Germany

Editorial responsibility: J. Hoefs

Introduction

The occurrence of chemical equilibrium between residue and melt is a fundamental assumption in petrogenetic studies of the formation of granitic melts (e.g. Hanson 1978). Unfortunately, inferred granitic melts can rarely be followed from the plutons back to their source region and, hence, chemical equilibrium or disequilibrium in the source region cannot be evaluated.

Partial melting can be best studied in anatexites, where former melts as well as residues are preserved. A fundamental problem in the geochemistry of anatexites as it pertains to granite genesis is the commonly observed discrepancy between element distribution in natural anatexites and in experiments. The high temperatures needed for partial melting make melt–residue equilibrium possible, but such equilibrium is rarely found. With few exceptions (e.g. Obata et al. 1994; Whitney and Irving 1994), most investigations documented that the composition of mineral phases in leucosomes and residues of anatectic rocks are similar. This is specially true for feldspar compositions (e.g. Misch 1968; Fitzsimonis 1996; Jung et al. 1998). In contrast, experiments show that plagioclase in the residues has a higher Ca/Na ratio than in the melt (Ashworth 1985; for a summary see also Johannes and Holtz 1996). The same discrepancy is found when comparing the trace element concentrations of minerals in leucosomes and melanosomes of migmatites (e.g. Bea et al. 1994).

In order to explain the unexpected compositional similarity of leucosome and residue in natural systems, different processes have been proposed (cf. Sawyer 1991; Johannes et al. 1995; Bea 1996; Watt et al. 1996; Sawyer 1998). This discussion must be subdivided into (1) achievement of residue–melt equilibrium during melting and (2) preservation of such an equilibrium during cooling and crystallization. Some authors, concerned about the achievement of equilibrium, have invoked disequilibrium melting (e.g. Johannes et al. 1995; Nabelek and Glascock 1995) in order to explain the final

composition. Others, concerned about the possible preservation of equilibrium compositions, attributed the similar trace element composition of melanosome and leucosome to mineral–mineral equilibrium formed during cooling and crystallization (Fourcade et al. 1992; Nabelek 1999). The latter studies observed a mineral–mineral re-equilibration with respect to trace elements, but a preserved mineral–melt equilibrium with respect to the major elements.

In order to understand the geochemical evolution of crustally derived, partially molten rocks, the parameters controlling the achievement and preservation of chemical equilibration or dis-equilibration must be investigated. Chemical equilibrium depends mainly on diffusion and/or surface-controlled processes. Both processes are time dependent at any given temperature and, therefore, related to the time interval of melting (e.g. Sawyer 1991). The effect of syn-magmatic deformation on the chemical composition of migmatites has received little attention in previous geochemical studies. However, dynamic recrystallization and/or deformation by diffusion creep may affect the chemical equilibrium of grains and melt. Diffusion creep in the presence of melt involves dissolution and re-precipitation, which destroy old mineral zoning and favour equilibration of grains with an interstitial melt. Dynamic recrystallization may also favour chemical exchange, as experimentally shown by Yund and Tullis (1991). In addition, melt infiltration along grain boundaries is also enhanced by deformation (Jin et al. 1994; Tullis et al. 1996; Rosenberg and Handy 2001), thus allowing a greater interaction between grains and melt.

The present paper presents a geochemical investigation of a syntectonic, partially molten metagranitoid. The well-preserved syn-magmatic microstructures of these migmatites allow us to distinguish areas where melt was present from areas that were melt-free (Rosenberg and Berger 2001). We, therefore, use microstructural criteria to discriminate between former melt and residues. We then make comparisons between the composition of microstructurally homogeneous rocks with the compositions of former residues and crystallized melts. Finally, we infer the operative deformation mechanisms, based on microstructural observations, and discuss their influence on chemical equilibration.

Geological setting and physical conditions of melting

The studied area is located in the Bergell Massif and represents the easternmost occurrence of Penninic nappes in the Central Alps (Fig. 1). A tectonic window exposes the floor of the Bergell tonalite and the underlying anatexites and gneisses that are described here. The same contact is also exposed along the western margin of the Bergell tonalite (Fig. 1; Rosenberg et al. 1995; Davidson et al. 1996).

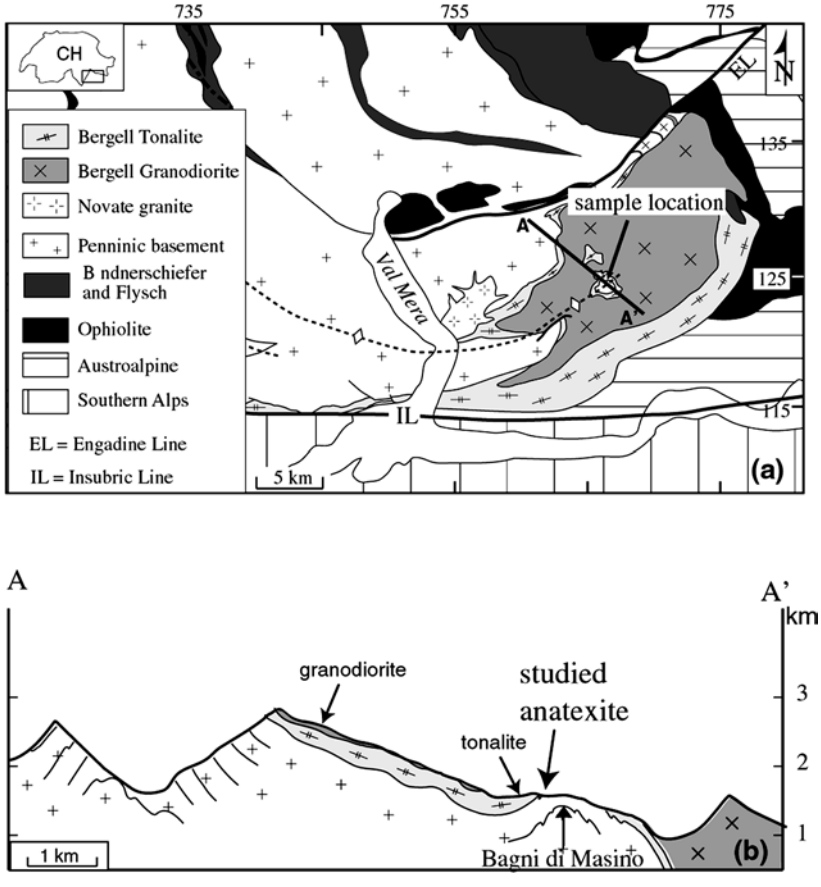

Fig. 1 **a** Simplified geologic map of Bergell area (central Alps; Switzerland–N Italy). Modified from Rosenberg et al. (1995). **b** NW–SE profile as indicated in **a** (modified from Davidson et al. 1996). The enclosing rocks of the Bergell pluton are exposed in a tectonic window, along the hinge of an antiform

The anatexites are directly in contact with the Bergell tonalite and partial melting is induced by the intrusion of the tonalite (Fig. 1). 'Al-in-hornblende' barometry indicates a pressure of 0.66 ± 0.04 GPa during crystallization of the tonalite (Davidson et al. 1996). Therefore, this pressure is inferred during partial melting in the contact aureole.

The temperatures for partial melting cannot be directly estimated because classical geothermometers for quartzo-feldspathic rocks are not available. Thermal modelling applied to the eastern contact of the Bergell pluton (Trommsdorff and Conolly 1996) suggests that a temperature of ~700 °C was achieved at the pluton's contact. Compared with the eastern margin, in our study area, the thickness of the tonalite is smaller and the pre-intrusive temperature of the country rock was higher (Davidson et al. 1996). These two parameters probably balance each other, suggesting that the peak temperature was about 700 °C or slightly higher. The occurrence of biotite in the residue and protolith indicates that melting did not involve this hydrous phase. Moreover, none of the expected anhydrous phases that form during biotite-dehydration melting are present. The absence of biotite dehydration melting gives an upper temperature limit of 760 °C for anatexis (Singh and Johannes 1996).

A temperature estimate based on zircon solubility in the leucosomes (Watson and Harrison 1983) yields temperatures between 704 and 780 °C for different leucosome compositions. The lower temperature (~700 °C) is consistent with the estimate above, whereas the upper temperature (780 °C) appears to be too high, because any solid product of incongruent biotite dehydration melting are missing. Note, however, that the use of Zr concentration as an geothermometer assumes that the investigated rock crystallized without solid particles as solid Zircon minerals. This is unlikely for most leucosomes.

However, these temperatures are sufficient for muscovite dehydration melting, but even in this case, none of the solid products of muscovite dehydration is found (i.e. sillimanite). Moreover, the protolith does not contain primary muscovite. Therefore, eutectic melting of plagioclase, quartz and K-feldspar must have been induced by the infiltration of a free aqueous fluid, most likely released by the crystallizing magmas of the Bergell pluton. An upper boundary for the duration of melting can be estimated from T–t paths typical for contact metamorphism (e.g. Hanson and Barton 1989). Given the P–T conditions discussed above, the solidus of the studied rocks was probably overstepped for no longer than 1 Ma.

Microstructures and deformation mechanisms

On the outcrop scale, the percentage of melting appears to have been higher in the vicinity of the pluton. The structurally lower unit, which is more distant to the pluton, consists of a K-feldspar-bearing augen gneiss and lacks any microstructural evidence for partial melting (e.g. Sawyer 1999). Closer to the pluton contact, centimetre-wide leucocratic veins, both parallel and discordant to the host foliation occur. Still closer to the contact the orthogneisses are progressively transformed into a heterogeneous rock with a weakly foliated granitic matrix, containing clasts of well foliated gneiss, varying from a few centimetres to approximately 50 cm across (Fig. 2a, b). Based on the mineral chemistry and the microstructures, we inferred that the augen gneisses represent the protolith, the leucocratic veins the segregated melt and the clasts the residues (Rosenberg and Berger 2001). The granitic matrix warping around the clasts was interpreted as a melt-crystal mush, which formed where melt did not segregate out of the rock. A detailed description of all these rock types and their microstructures may be found in Rosenberg and Berger (2001). Here, we will only describe the relevant microstructures of the clasts and of their granitic matrix.

On the scale of a thin section, clasts have a banded structure consisting of alternating monophase aggregates of quartz, plagioclase and biotite (Fig. 2c), which form a pronounced foliation. Quartz grains are elongate, they have lobate grain boundaries, undulose extinction, subgrains and deformation bands, suggesting that quartz deformed by dislocation creep associated with grain boundary migration recrystallization. Plagioclase grains also have lobate grain boundaries, folded twin planes and a weakly elongated shape (Fig. 2d). Hence, flow of plagioclase also occurred by crystal plasticity associated with dynamic recrystallization. Biotite forms elongate aggregates and the (001) plane of most grains is parallel to the foliation.

In the granitic matrix, interphase boundaries are more randomly distributed, i.e. the existing phases do not concentrate into bands of monophase aggregates (Fig. 2e). K-feldspar is present in these rocks, there is no evidence for a competence contrast between the different minerals, and only the shape-preferred orientation of anisotropic grains defines a weak foliation. Biotite grains do not form interconnected layers, nor aggregates. Most biotite grains are isolated, and their (001) planes do not show a pronounced preferred orientation parallel to the foliation. Intergranular films of K-feldspar, quartz and biotite commonly coat the boundaries between quartz and plagioclase grains (Fig. 2f). Following the interpretation of Rosenberg and Riller (2000) and Sawyer (2001), we infer that these films crystallized from an intergranular granitic melt.

The lack of competence contrast between minerals and the weak or absent shape preferred orientation in the granitic matrix suggest that deformation occurred by granular flow, i.e. by sliding of grains past each other, grain shape readjustments and dissolution and re-precipitation (e.g. Paterson 1995, 2001). Deformation by this mechanism does not create elongated grain shapes nor interconnected monophase bands. In fact, in the absence of strain markers, the microstructure of a rock that was deformed by granular flow may be difficult to

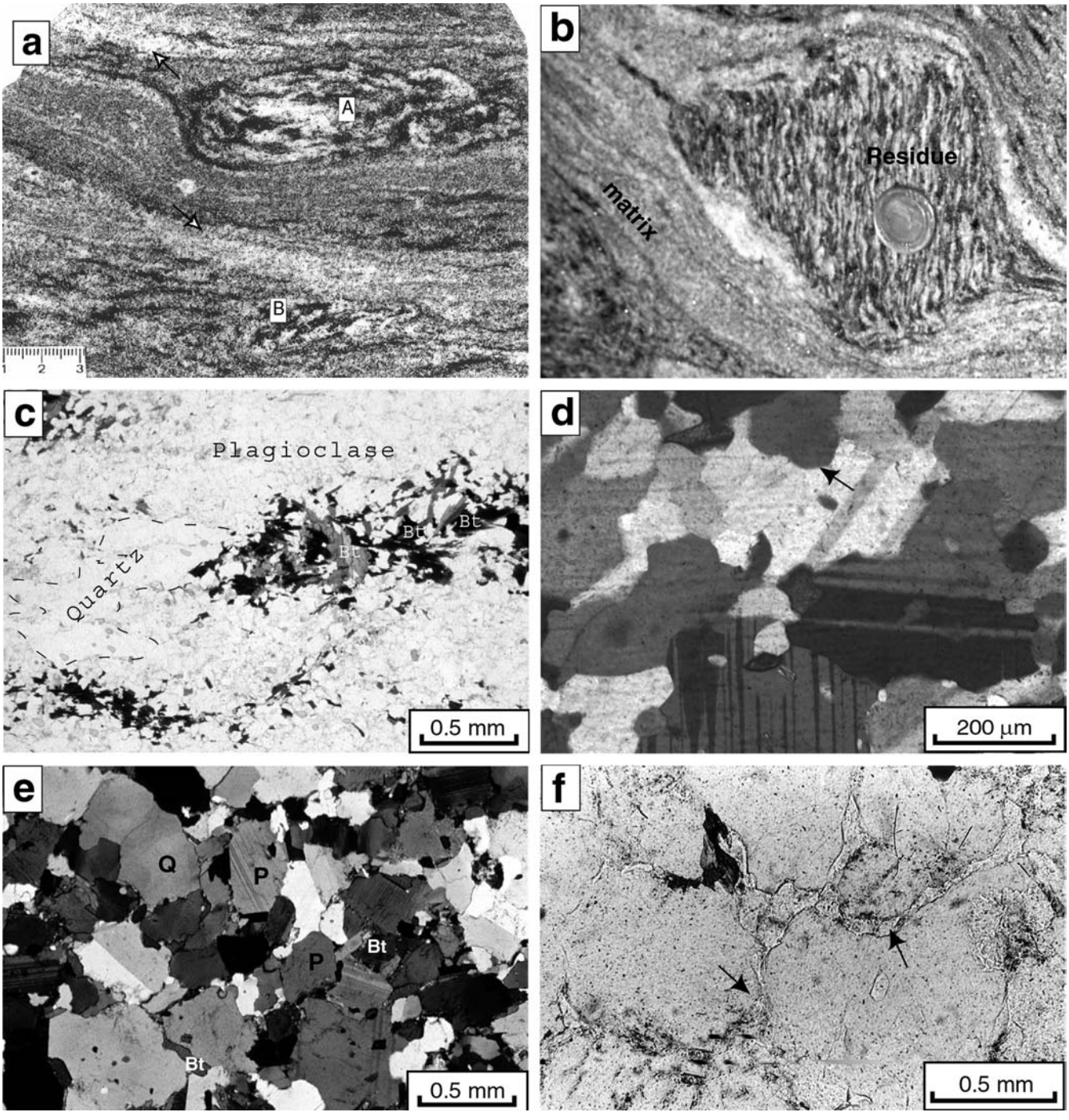

Fig. 2a–f Photographs and microphotographs of the investigated samples. **a** Hand sample showing a gneissic clast (*A*) in a matrix. Note the occurrence of residue material; (*B*) with diffuse contact with the matrix. *White arrows* indicate foliation parallel leucocratic veins. **b** Residue consisting of a competent clasts in the granitic matrix. Note the intense foliation of the clast in contrast to the matrix. **c** Plane light microphotograph of a residual clast. Note the layered arrangement of quartz aggregates, plagioclase aggregates and biotite aggregates, which form the foliation of this rock. **d** Plagioclase aggregate in a residual clast. Note the lobate grain boundaries, suggesting dynamic recrystallization by grain boundary migration. **e** Part of the matrix deforming by melt-present granular flow. Note the lack of monomineralic aggregates and the weak shape preferred orientation of all mineral phases (*Q* quartz; *P* plagioclase; *Bt* biotite). **f** Photomicrograph of intergranular K-feldspar film (see *black arrow*)

distinguish from the microstructure of an unstrained rock. We infer, however, that deformation was in fact concentrated in the matrix because it wraps around the more competent clasts (Fig. 2).

Mineral and bulk rock chemistry

Analytical methods

The major elements in plagioclase and biotite were measured with an electron microprobe Cameca SX50. We used silicate standards, an acceleration voltage of 15 kV, a beam current of 10 mA and a

Table 1 Mineral chemistry of plagioclases. Additionally, An contents from whole-rock analysis are presented using CIPW norm

	BM17 (Residue)	C9947 (Leuco)
SiO_2	58.39	60.47
Al_2O_3	26.69	23.40
CaO	7.9	5.41
Na_2O	7.25	8.37
K_2O	0.26	0.351
Sum	100.62	98.08
Si	2.588	2.74
Al	1.394	1.249
Ca	0.375	0.263
Na	0.623	0.735
K	0.015	0.02
*X*An	0.37	0.26
*X*Ab	0.61	0.72
*X*Or	0.015	0.02
An aus CIPW	34	24

counting time of 20 s. The raw data were corrected using PAP procedures. Trace elements in biotite and feldspars were determined with a μ-XRF (Cheburkin et al. 1997). The spatial resolution of the μ-XRF was 35 μm, nearly one order of magnitude smaller than the mean grain size (100–500 μm). Absolute concentrations could not be determined because the necessary standards were not available. However, relative comparisons can be made. Counting times varied between 20–40 min per analysis using a primary Mo-tube operating at 45 kV and 20 mA. Major elements and Sr, Rb, Ba, Pb, Ni, V, Zr, Zn and Y in bulk rock were determined by standard X-ray fluorescence on glass pellets.

Mineral chemistry of leucosome, matrix and residue

The anorthite content of plagioclase in the matrix and in the leucosomes ranges between An28 and An25. In contrast, the composition of plagioclase in the residues ranges between An37 and An44 (Table 1). Intragranular compositional variations in plagioclase are small. μ-XRF analyses indicate that the feldspars are the main carriers of Sr, and to a minor extent of Rb and Fe.

The *X*Mg (= Mg/Mg + Fe) of the biotite grains varies systematically between the residues, the protoliths and the leucosomes (Table 2, Fig. 3). The slight change in Fe/Mg ratio in biotite occurs in combination with the growth of Fe- and Fe–Ti oxides. The different *X*Mg values do not result from a temperature variation, as indicated by the constant Ti content of biotite in all samples investigated. Small variations of Ti-content within one sample are locally caused by exsolution of ilmenite. The trace elements in biotite are mainly Zn and Rb.

Whole-rock chemistry

Microstructurally homogeneous parts of the hand specimens (i.e. homogeneous modal composition and microstructures pointing to the same dominant deformation mechanism) were selected with care. Hence, the sample-volumes were sometimes small. The data are presented in several co-variation diagrams (Figs. 4, 5 and 6, Table 3). This discrimination of the anatexite parts is based on structural/microstructural observations. However, different degrees of melt segregation in some of the matrix samples is responsible for the spread of chemical data.

Table 2 Mineral chemistry of biotite

Sample	C9946 (Residue)	C9947 (Leuco)
SiO_2	34.895	34.368
Al_2O_3	15.652	16.943
TiO_2	3.444	3.766
FeO	20.947	21.335
MnO	0.406	0.339
MgO	9.833	8.032
CaO	0.016	0.054
K_2O	9.71	9.598
Na_2O	0.092	0.103
F	0.526	0.665
H_2O (calc)	3.581	3.492
Sum	99.105	98.695
On the base of 32O		
Si	5.920	5.861
Al (tot)	3.130	3.405
Ti	0.440	0.483
Fe	1.320	1.777
Mn	0.058	0.049
Mg	2.487	2.042
Ca	0.003	0.010
Na	0.030	0.034
K	2.102	2.088

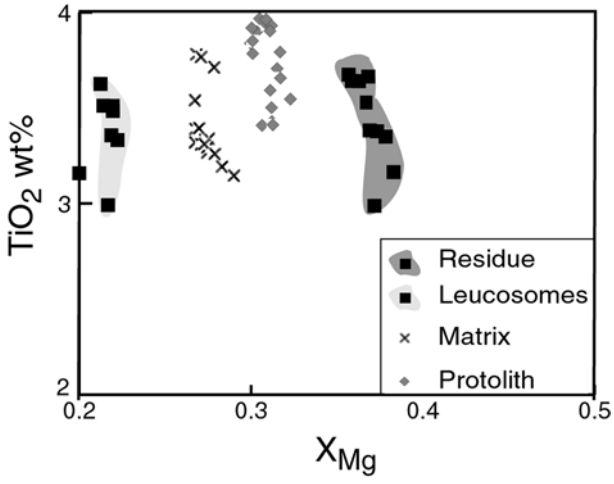

Fig. 3 Composition of the biotite in different parts of the anatexites. Note the similar TiO_2 content at variable *X*Mg [= Mg/(Mg + Fe)]

The transition metals

The Mg/Fe ratio of the whole rock does not change systematically in the different rock types (Fig. 4). In contrast, the transition metals (e.g. Ti, V, Zn) increase from leucosomes to restites (Fig. 5). As shown by in-situ μ-XRF analyses (see before), biotite is the main carrier of the transition metals (i.e. Ti, Zn). These trace

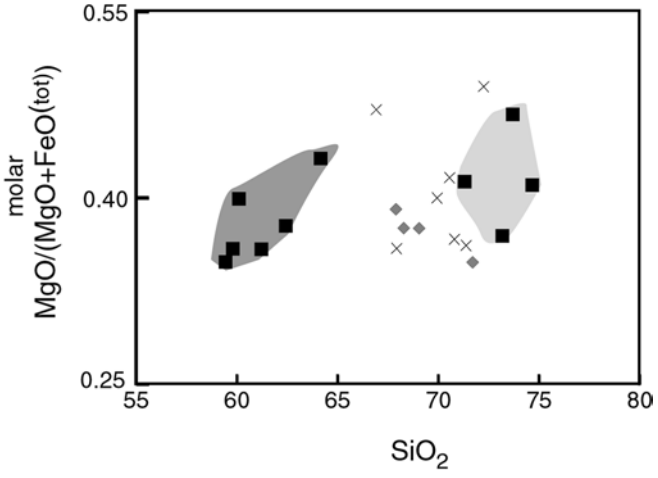

Fig. 4 Co-variation diagrams of the bulk-rock chemistry between $Mg/(Mg+Fe^{tot})$ versus SiO_2. *Symbols* are the same as in Fig. 3

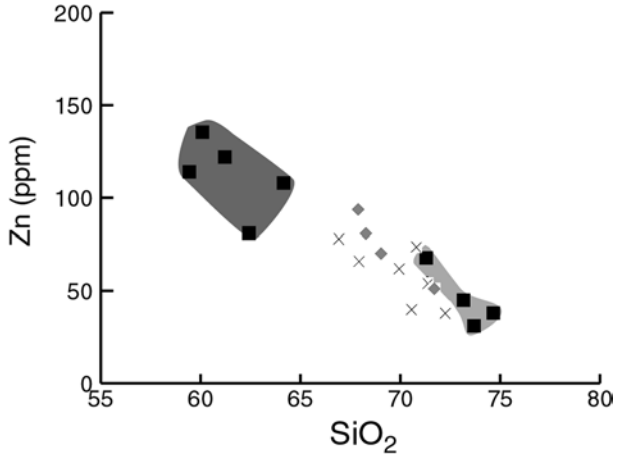

Fig. 5 Co-variation diagrams for Zn versus SiO_2. *Symbols* are the same as in Fig. 3

elements are expected to be partitioned into biotite during partial melting (see Mahood and Hildreth 1983; Nash and Crecraft 1985; Green 1994 for a review). No other main rock-forming phase contains any transition metals and, therefore, no significant changes of trace element concentrations in biotite are expected. In summary, the total amount of transition metals is simply related to the abundance of biotite in the sample. This behaviour of the transition metals is expected to be markedly different under conditions of biotite dehydration melting (Sawyer 1998).

The alkali and alkali earth elements and the behaviour of feldspars

Feldspars are the main carriers of Ca, Na, Pb and Sr. The chemical distribution of these elements is essential to understanding geochemical transfers during partial melting. Controversies about the generation of partial

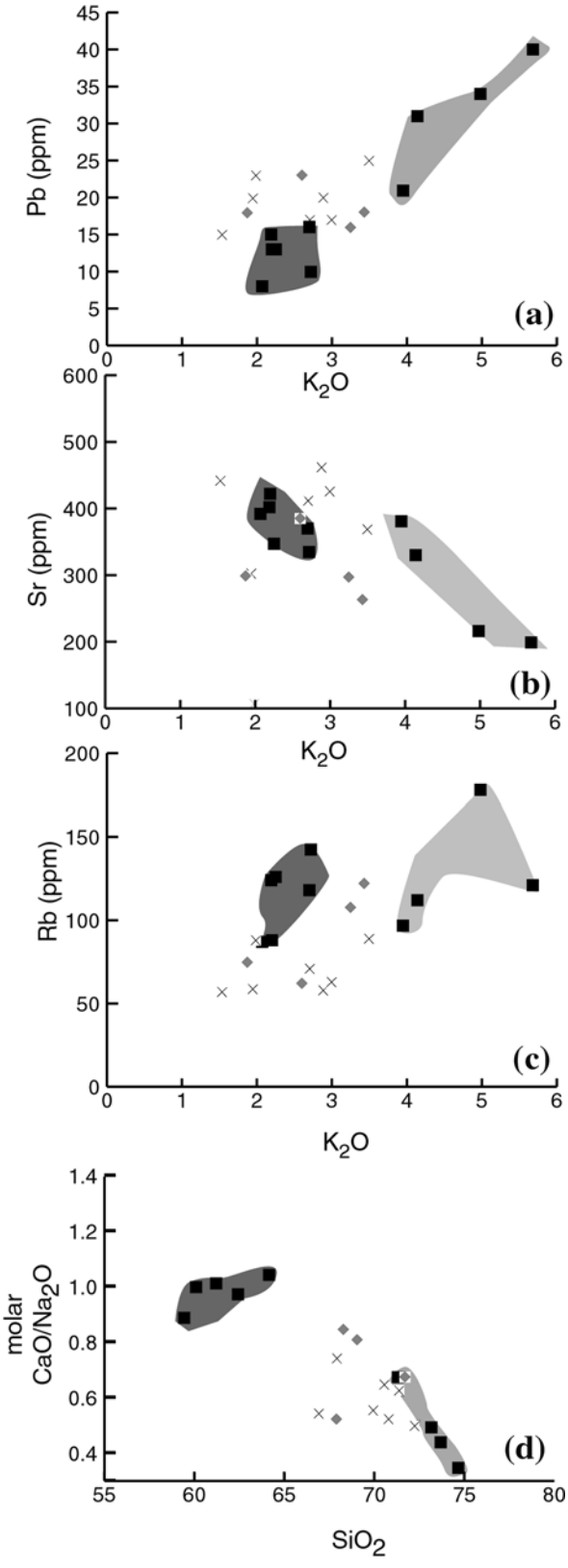

Fig. 6 Co-variation diagrams for different elements: **a** Pb versus K_2O; **b** Rb versus K_2O; **c** Sr versus K_2O; **d** CaO/Na_2O versus SiO_2. *Symbols* are the same as in Fig. 3. See text for discussion

Table 3 Representative XRF analysis of matrix, residue and protolith samples

	Matrix			Leucosomes			Residues					Protolith		
	BM23	BM18	BM 16	BM5	BM22	BM15	BM24	BM25	BM6	BM17/2	C9949	BM7	BM8	C9950
SiO_2 (wt%)	69.92	70.54	72.23	73.17	74.66	73.69	62.42	61.21	59.43	59.79	67.89	71.70	69.04	68.28
TiO_2 (wt%)	0.34	0.29	0.19	0.20	0.07	0.16	0.66	0.82	0.88	0.94	0.52	0.21	0.46	0.49
Al_2O_3 (wt%)	15.63	15.36	14.40	14.59	13.78	13.63	17.61	18.07	19.18	18.04	16.84	15.55	14.85	16.09
Fe_2O_3 (wt%)	2.40	2.02	1.24	1.62	0.54	1.06	4.61	5.92	6.07	5.98	3.99	1.63	3.38	3.64
MnO (wt%)	0.02	0.03	0.02	0.04	0.01	0.02	0.07	0.11	0.09	0.08	0.06	0.03	0.06	0.06
MgO (wt%)	0.81	0.73	0.60	0.48	0.19	0.47	1.41	1.67	1.64	1.69	1.29	0.44	1.03	1.11
CaO (wt%)	2.27	2.42	2.24	1.70	1.02	1.34	3.93	4.10	4.10	4.19	3.00	2.65	2.71	3.11
NaO (wt%)	4.55	4.16	4.99	3.80	3.24	3.36	4.47	4.47	5.11	4.67	6.34	4.35	3.71	4.06
K_2O (wt%)	2.88	2.99	1.98	4.14	5.68	4.98	2.70	2.25	2.19	2.20	1.87	2.60	3.43	3.25
P_2O_5 (wt%)	0.05	0.10	0.11	0.07	0.08	0.14	0.54	0.31	0.28	0.33	0.06	0.05	0.16	0.16
LOI (wt%)	0.46	0.28	0.18	0.21	0.23	0.34	0.43	0.34	0.44	0.35	0.48	0.25	0.35	0.39
Sum	99.46	99.12	98.18	100.18	99.60	99.28	99.01	99.43	99.58	98.26	102.45	99.63	99.30	100.8
Ba (ppm)	633.08	1371	176.67	1097.	585.67	403.61	664.14	446.45	499.79	799.12	251.8	978.5	700.5	916.4
Nb (ppm)	12.94	6.98	11.98	7.98	5.99	11.96	22.90	24.91	19.91	21.92	9.95	7.98	10.96	11.95
Pb (ppm)	19.91	16.95	22.96	30.94	39.91	33.88	15.93	12.96	14.93	12.95	17.92	22.94	17.94	15.94
Rb (ppm)	57.73	62.82	87.84	111.77	120.73	178.39	118.49	125.56	124.45	87.68	74.65	61.85	121.57	107.59
Sr (ppm)	461.87	425.81	106.80	330.32	198.55	216.26	370.40	346.80	402.22	422.48	298.60	385.05	263.06	296.86
V (ppm)	19.91	34.90	13.97	18.96	4.99	11.96	66.71	81.72	77.66	73.73	47.78	20.95	48.83	43.83
Y (ppm)	10.95	14.96	12.98	17.96	29.93	9.97	60.74	55.81	37.83	44.84	24.88	11.97	25.91	18.93
Zn (ppm)	61.72	39.89	37.93	44.91	37.91	30.89	80.65	121.58	114.49	114.59	93.56	50.87	69.75	80.69
Zr (ppm)	194.10	150.58	164.69	136.72	68.84	96.67	290.75	383.67	371.36	365.68	266.75	151.62	215.23	256.02

melts are to a large extent based on differences between feldspars grown experimentally and feldspars in anatexites (cf. Ashworth 1985; Sawyer and Barnes 1988).

In our samples, Sr shows a negative correlation with K_2O (Fig. 6), in contrast to most data on anatexites reported in the literature (e.g. Bea et al. 1994; Nabelek 1999). Sr has a high partition coefficient (KD) for both feldspars (Green 1994; Icenhower and London 1996). Therefore, Sr is expected to be enriched into the solid residue and not into the melt. Pb contents show a weak correlation with K_2O, and a negative correlation with CaO. Based on experimentally-derived KD values, Pb is expected to be partitioned into K-feldspar (Nash and Crecraft 1985). The initial volume of K-feldspar is consumed during melting and only a small portion of the Pb will distribute into the plagioclase. Therefore, most of the Pb is expected to concentrate into the melt if K-feldspar is absent from the residue. In our samples, the highest concentrations of Pb are in the leucosomes, whereas the lowest concentrations are in the residues (Fig. 6). This type of final concentration of Pb could also be explained by mineral–mineral equilibria because no significant difference is expected between plagioclase–melt equilibria and plagioclase–alkali-feldspar equilibria. Therefore, Pb cannot be used to discriminate between achievement and preservation of mineral–melt and mineral–mineral equilibria.

The Ca/Na ratio of the whole rock and the Ab/An ratio of the plagioclase grains in residue and leucosome vary systematically (Fig. 6, Table 1). As expected, the An content of plagioclase is low in the leucosomes and the highest in the residues. These data suggest equilibration of residual plagioclase grains with the melt. This is particularly important because the Ca/Na ratio in plagioclase is controlled by the coupled exchange ($CaAlNa_{-1}Si_{-1}$), which is very slow (e.g. Yund 1986; Bascheck and Johannes 1995). The equilibration of the feldspars is also demonstrated by the minimum melt composition of the segregated melts (Fig. 7). The minimum melt composition also indicates high water activities, as already inferred from petrological consideration.

In order to quantitatively evaluate the existence of melt–residue equilibrium, the distribution of Sr between melt and minerals was modelled, using the batch melting equation (e.g. Langmuir et al. 1992). Major parameters by modelling partial melting is the melt fraction (F) and the bulk distribution coefficient of an element (D), which result from the sum of the mineral fractions of all minerals and their related KD values . The mineral fractions are estimated by point counting

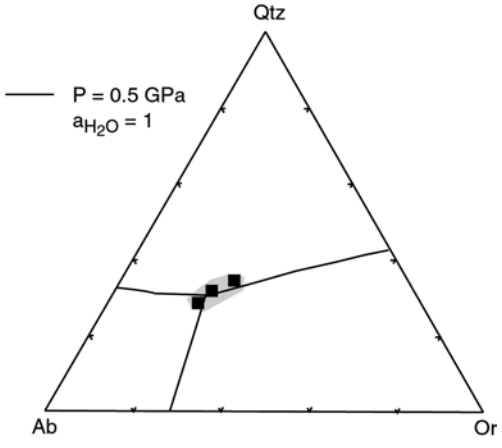

Fig. 7 Qtz–Ab–Or triangular plot. The cotectic lines at water activity of 1 are included (taken from Johannes and Holtz 1996). Normative composition of the measured leucosomes are plotted, which show nearly perfect minimum melt compositions

of thin sections. We calculated F by optimizing the K_2O content between protolith and residue composition, using the given leucosome composition. This calculation results in a segregated melt fraction of 0.32 for the residue that lost the greatest melt fraction. However, the melt fraction equilibrated for each sample are impossible to estimate, and we computed models for melt fractions between 0 and 0.5 (Fig. 8). For the calculated melt fraction, the measured leucosome Sr concentration are slightly above the modelled data. In addition, values for the intermediate samples (granitic matrix) show a large spread. However, the measured composition of the residues is in good agreement with the modelled distribution at F = 0.32 (Fig. 8). The Sr concentrations in leucosome and residue of the Bergell anatexite are consistent with a batch melting model (Fig. 8).

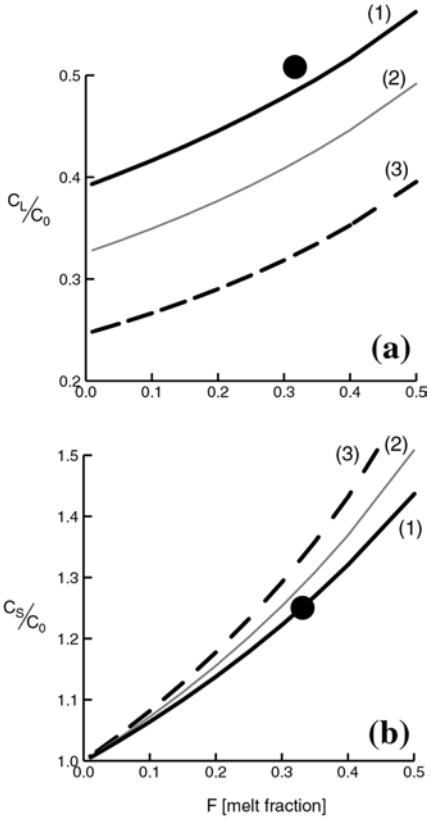

Fig. 8 Modelling of strontium concentrations during batch melting. Model 1 assumes equilibration between the residual minerals observed in the residues and the melt (mineral fractions are Plag = 0.55; Bt = 0.3). KD of plagioclase are taken from Arth (1976) and for biotite from Nash and Crecraft (1985). Model 2 uses the modal abundance of the protolith (mineral fractions are Plag = 0.45; Kfs = 0.2; Bt = 0.13) with the same KD values as model 1, and additionally alkali-feldspar from Nash and Crecraft (1985). Model 3 is identical to model 2, but with KD values for alkali-feldspar from Icenhower and London (1996). In addition, the measured values are shown as *dots* for F = 0.32, which is calculated for the most segregated residue. C_L/C_o is the concentration ratio between the melt and the start material; C_S/C_o is the concentration ratio between the residue and the start material

The rare earth elements (REE) and the accessory minerals

We analysed the REE concentrations by ICP-MS in six samples (analysed in the Activation Laboratories, Canada; Table 4). The bulk REE content is the lowest in the leucosomes, whereas it is the highest in the residues (Fig. 9). In order to investigate the potential differentiation of the REE's, we normalized the REE contents of the six samples to the content of the protolith (Fig. 9). The grey area in Fig. 9 indicates the variation of the protolith defined by two samples. The residue shows an increase in heavy rare earth elements (HREE) in comparison to the protolith. The two leucosomes show different trends in this normalization. The composition of one leucosome clearly reflects a counterpart to the residue. The distribution of the REEs and some other high field strength elements (i.e. Y, Zr, Hf) depends on the behaviour of their main host accessory minerals.

The accessory minerals in the protolith are mainly allanite, zircon and minor apatite. The allanite is up to 0.7 mm in size and some crystals are weakly zoned. The leucosomes contain no allanite, but rare apatite, zircon and monazite. The residues are dramatically enriched in apatite, monazite and zircon. Some rare residues also contain allanite, but these grains are smaller than in the protolith. The occurrence of monazite both in the leucosome and in the residue suggests a mineral reaction during partial melting because monazite is a newly-formed mineral that is absent in the protolith. The absence of allanite in most of the residue suggests that allanites were consumed during partial melting. Therefore, allanite was not inert during partial melting, so that the hosted REE could have reached equilibrium.

Zr and Hf decrease systematically with increasing SiO_2 content. This chemical correlation could result from enrichment of zircons in the residue or from equilibration of Zr between melt and zircon minerals. In order to discriminate between these possibilities, a mass balance calculation is done for variable melt fractions

Table 4 REE analysis of structurally selected proportions of the anatexites

	Leucosome		Residue	Matrix	Protolith	
Sample	C9947	BM5	BM17/2	BM23	BM8	C9950
La (ppm)	41.97	42.56	58.97	54.65	49.59	55.96
Ce (ppm)	85.04	85.72	122.55	110.80	98.38	111.97
Pr (ppm)	8.82	8.68	13.34	10.96	9.64	11.45
Nd (ppm)	36.20	35.21	55.25	43.40	36.25	44.01
Sm (ppm)	6.27	6.92	11.22	7.55	6.79	7.15
Eu (ppm)	1.72	1.22	2.36	1.55	1.18	1.47
Gd (ppm)	5.13	5.53	9.97	4.75	5.45	5.57
Tb (ppm)	0.68	0.81	1.58	0.52	0.87	0.74
Dy (ppm)	2.71	3.86	7.75	1.94	4.43	3.43
Ho (ppm)	0.38	0.74	1.40	0.27	0.78	0.56
Er (ppm)	0.85	2.47	4.24	0.68	2.26	1.58
Tm (ppm)	0.09	0.41	0.64	0.10	0.35	0.22
Yb (ppm)	0.49	2.80	3.99	0.64	2.19	1.26
Lu (ppm)	0.05	0.41	0.57	0.08	0.33	0.16

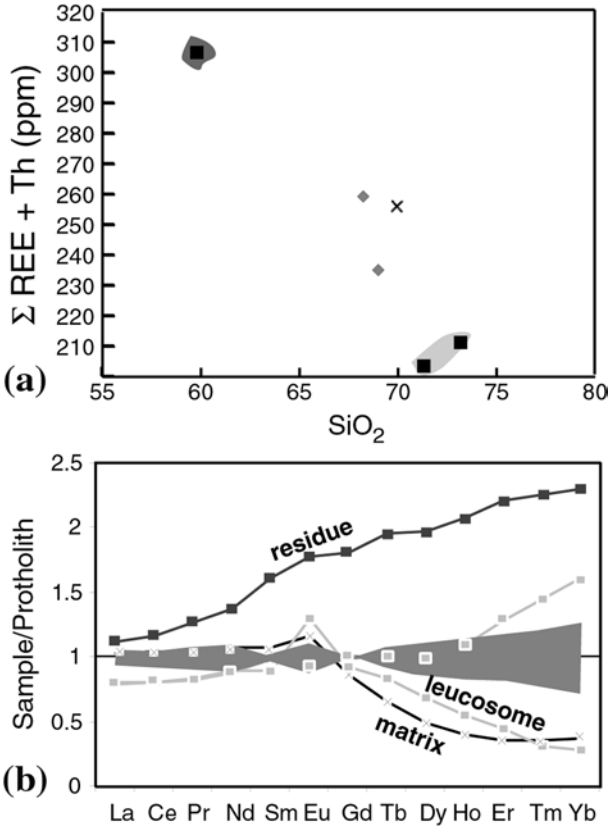

Fig. 9 Behaviour of elements hosted by accessory minerals. **a** Sum of REE + Th against SiO_2. Notice the enrichment of REE in the residue. *Symbols* are the same as in Fig. 3. **b** Spider diagram of the REE normalized to the average of the protolith. The *grey area* represent the variations of the protolith composition

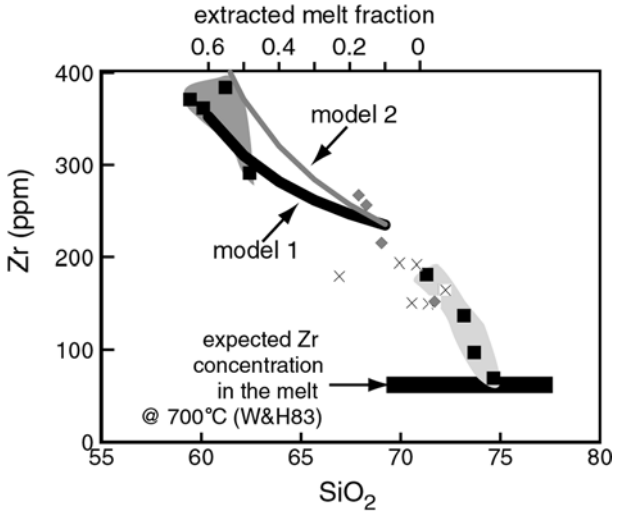

Fig. 10 Element distribution of zircon between leucosome and residue. Measured data are shown as *individual symbols* (*symbols* are the same as in Fig. 3). Additionally, mass balance calculations are done by extracting different melt fractions from an average protolith. The expected residue should contain certain SiO_2 contents. Therefore, the melt fraction is presented on top of the diagram, which is connected with a certain SiO_2 content. Model 1 uses the extraction of melt with 68 ppm Zr and model 2 uses the same calculation with 137 ppm Zr in the melt. In addition, the theoretical Zr saturation concentration is calculated from Watson and Harrison (1983; = W&H83) using a temperature of 700 °C and a water content of 6.5 wt%

and variable Zr content in the melt (solid lines in Fig. 10). The observed Zr concentration can be explained by the extraction of relative high melt fractions (F ~0.5; Fig. 10). As pointed out in the geological setting, the lowest Zr concentration are consistent with expected values by solution of Zr in the melt. However, segregation of pure melt may be unlikely for most leucosomes.

Discussion

Trace element distribution between residues and leucosomes measured in natural anatexites often differ from the concentrations calculated using experimentally derived KD values. Three factors may explain this discrepancy: first, mineral–melt equilibrium is not achieved in natural anatexites. Second, during cooling and crystallization, mineral–mineral equilibrium overprints and deletes any previously achieved mineral–melt equilibrium. Third, mineral–melt equilibrium is achieved in natural rocks, implying that most KD's are close to 1 (Bea et al. 1994).

In the Bergell anatexites, major and trace element distributions of several elements are consistent with those expected from experiments. For example, Sr has a high partitioning coefficient (> 1) for both feldspars in equilibrium with a granitic melt (e.g. Green 1994). Therefore, Sr is expected to be enriched into the solid residue and not in the melt. Indeed, the Sr-content decreases in the rocks inferred to have crystallized from the melt (Fig. 6), even though they contain K-feldspar-rich leucosomes, because biotite and plagioclase act as sinks for Sr during initial melt–residue equilibrium. In contrast, most examples in the literature (e.g. Bea et al. 1994; Nabelek 1999) report a positive correlation of Sr with K_2O content, which are generally high in leucosomes and low in residues. This indicates that late mineral–mineral equilibration instead of mineral–melt equilibria may have controlled the distribution of some trace elements in the anatexites of the latter investigations.

The present work shows that equilibrium, residue/melt distributions of major and trace elements can apparently be achieved and preserved under some natural conditions. This interpretation is supported by most of our chemical data. (1) The leucosomes have a minimum melt composition (Fig. 7). (2) The anorthite component of plagioclase increases in the residue and decreases in the leucosome (Table 1). (3) Sr is enriched in the residue and lowest in the leucosome. (4) The different microstructures observed in the residue and protolith, on the one hand, and in the leucosome and the granitic matrix, on the other hand, are typical for melt-absent and melt-present deformation, respectively.

The fact that the distribution of the HREE between the leucosome and residue does not reflect the expected equilibrium between melt and residue is not a contradiction of the above interpretation. It merely shows that the attainment of an equilibrium distribution for a given element is also dependent on the behaviour of its host mineral. The HREE are hosted in the xenotime/zircons that can be refractory during partial melting. As a consequence, equilibrium distribution of HREE may not be achieved. We argue that two main factors contributed to the formation and the preservation of the observed distributions. Deformation enhanced chemical equilibrium between residue and melt, and rapid cooling under contact metamorphic conditions, inhibiting mineral–mineral re-equilibration (e.g. Nabelek 1999). We suggest that only in relatively fast cooling and crystallizing anatexites are mineral–melt equilibria preserved.

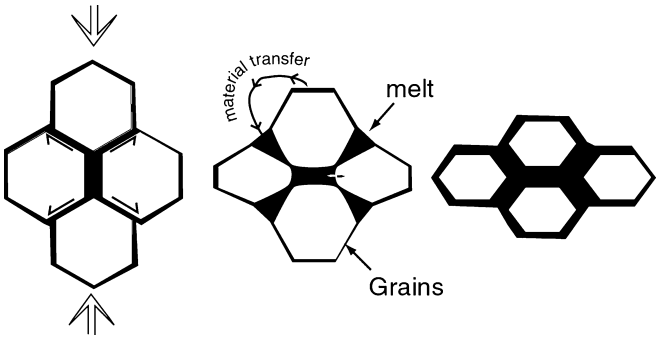

Fig. 11 Schematic drawing of processes active during melt present granular flow. Granular flow includes grain boundary sliding and transfer of material from local high stress sites to low stress sites. In the case of melt presence, this transport occurs via local melting and re-precipitation

The effect of deformation on chemical equilibrium

We believe that deformation enhances chemical equilibrium mainly in two ways: by inducing dynamic recrystallization in the residue, and by activating diffusion-accommodated grain boundary sliding in the granitic matrix. We inferred above that the clasts of the residue were deformed by dislocation creep involving grain boundary migration recrystallization (see Fig. 2). As experimentally demonstrated for plagioclase aggregates (Yund and Tullis 1991), this recrystallization mechanism enhances the exchange of elements between mineral grains and fluid in a rock. Na/Si and Ca/Al exchanges occur by diffusion along the high-angle grain boundaries that sweep through a work-hardened grain. This process may be responsible for a continuous compositional change of the residue.

The granitic matrix deformed by granular flow in the presence of melt (see the section Microstructures and deformation mechanisms). This process involves dissolution of material into the melt and re-precipitation on solid material and permanent switching of neighbouring grains (e.g. Paterson 1995, 2001; Fig. 11). Thus, enhancing mineral–melt equilibrium mainly in two ways: (1) continuous movement, by gliding of grains past each other minimizes transport distances (Fig. 11); and (2) deformation-induced dissolution and precipitation causes the dissolution of large portions of the solid rock, even if melt fractions are low.

To (1): Reaction kinetics and their progress are controlled by the size of local chemical overstepping (high chemical overstepping enhance reaction progress). However, under static conditions, chemical gradients decrease during ongoing reaction progress. In a material deforming by sliding of grains past each other, continuous switching of neighbouring grains (Fig. 11) may enhance the maintenance of high chemical gradients during ongoing reactions. In addition, mechanical movements of grains (and melt) shorten the transport distance of chemical components.

To (2): The transport of chemical components by dissolution and precipitation is more effective than by pure diffusion of cations through solids and melt. This interpretation is also supported by experimental data, indicating that the process of solution and precipitation has a larger effect on equilibration than pure diffusional transfer (Johannes et al. 1994). In addition, components solved in the melt can be transported by convection.

During diffusion-accommodated grain boundary sliding, provided that finite deformation is large, the entire volume of the solid rock may become dissolved into the melt (not at the same time), irrespective of the small melt fraction.

The role of chemical parameters on the equilibrium of the REE's

The attainment of chemical equilibrium for elements hosted in the rock-forming minerals depends on the reaction kinetics of these minerals. The accessory phases are affected similarly, but their stability in different chemical systems is less known. Previous studies suggest that REE's and high field strength elements rarely reach equilibrium during crustal melting due to the refractory behaviour of their host minerals (e.g. Nabelek and Glascock 1995; Bea 1996; Watt et al. 1996). In contrast, the Bergell samples show a reactive behaviour of some accessory minerals. The occurrence of allanite in the protolith versus the occurrence of monazite in residue and leucosome suggests the reactive behaviour of allanite during partial melting and melt segregation. The parameters controlling stability of these phases are P, T, a_{Ca}, f_{O2} and/or a_{H2O}. However, the f_{O2} and a_{H2O} are coupled by the dissociation of water. P and T did not vary substantially between leucosome, residue and protolith because all these rock types can be found on one and the same outcrop.

In the leucosome, as well as in the residue, monazite is the main carrier of LREE. The concentration of LREE's is high both in allanite and in monazite,

although the major element composition of these minerals is different. The activity of some of these major elements is suggested to control the stability of allanite vs monazite. For example, Ca activity controls the stability of allanite, implying that monazite develops at low a_{Ca} (e.g. Casillas et al. 1995; Broska et al. 2000 and discussion therein) However, leucosomes and residues differ substantially in their Ca concentration (Fig. 6), which is markedly higher within the residue. Nevertheless, monazite is stable in the residue, suggesting that Ca activity is not the only factor controlling the stability of monazite.

Water activity changes during water-present melting and crystallization (e.g. Holtz et al. 1996; Johannes and Holtz 1996). Water activity is low as long as water is solved in the melt (also during water-present melting). The residue and leucosome preserved these conditions of low water activity, which may have stabilized monazite over allanite also in Ca-rich parts of the rocks. The change of phase stability between the protolith and the neosomes induced a change in the concentrations of the LREE in the bulk samples. Therefore, we assume equilibration for the LREE. In low aluminium-saturated index (ASI) melts and at temperatures near 700 °C, the solubility of ΣREE is low (e.g. Montel 1993; see also Johannes and Holtz 1996). Using the equation of Montel (1993), we expect ΣREE of 72 ppm at 700 °C and water contents of 6.5 wt% in the melt. The measured concentrations of ~190 ppm (=ΣREE) exceed this theoretical value. This may be related to the behaviour of the HREE-containing minerals (see also Zr concentration in leucosomes). They may have a more refractory behaviour in comparison to the allanite. The different behaviour of the accessory minerals also influences the REE pattern of the partially molten rocks and residues. The residue shows an enrichment of HREE, whereas the LREE shows similar patterns in protolith, residue and leucosome (Fig. 9).

Concluding remarks

The results of the present study suggest that (1) under natural conditions, chemical equilibrium of several major and trace elements can occur between melt and residue, (2) such equilibrium can be preserved through cooling and crystallization, and (3) major and trace element distributions in natural anatexites are not necessarily close to 1 and experimental KD values are useful values.

The microstructures of the deformed anatexite indicate that granular flow is the dominant deformation mechanism where melt is present in the system. During deformation, different degrees of melt segregation occur, as evidenced by the chemical signature of the investigated samples. All samples representing the matrix of the residual clasts show chemical compositions ranging between residues and segregated melt. This variation reflects the chemical preservation of different amount of melt segregation during partial melting and segregation. In addition, the occurrence of inferred interstitial melt films suggests that the 'partially molten stage' is preserved in the microstructure of the investigated rocks. The preservation of both chemical and microstructural signatures of melting probably results from fast cooling and crystallization in the contact metamorphic aureole. This is consistent with other examples of contact metamorphic aureoles showing the preserved microstructural signature of former melt (e.g. Holness and Clemens 1999; Rosenberg and Riller 2000).

The absence of late mineral–mineral equilibration allows us to test experimental and theoretical considerations on diffusion, especially in feldspars. It is generally considered that diffusion rates are too slow to equilibrate rocks in geological time intervals (e.g. Johannes and Holtz 1996 and literature therein). In contrast, the present study suggests that repeated reaction between mineral and melt can occur as a result of deformation-induced dissolution and continuous switching of neighbouring grains. Therefore, we may expect chemical equilibration between melt and residue to occur in most areas affected by syntectonic anatexis.

Acknowledgements We thank P. Nabelek and an anonymous referee for very helpful reviews. C.R. greatly acknowledges funding from the Deutsche Forschungsgememeinschaft (Ro 2177/1-1) and A.B. from Schweizerischer Nationalfond (20-63593.00). We thank E. Gnos for additional microprobe analysis.

References

Arth JG (1976) Behaviour of trace elements during magmatic processes – a summary of theoretical models and their applications. J Res US Geol Surv 4:41–47

Ashworth JR (1985) Introduction. In: Ashworth JR (ed) Migmatites. Blackie, Glasgow, pp 1–31

Bascheck G, Johannes W (1995) The estimation of NaSi–CaAl interdiffusion rates in peristerites by homogenization experiments. Eur J Mineral 7:295–307

Bea F (1996) Residence of REE, Y, Th and U in granites and crustal protoliths; implications for the chemistry of crustal melts. J Petrol 37:521–552

Bea F, Pereira MD, Stroh A (1994) Mineral/leucosome trace element partitioning in a peraluminous migmatite (a laser ablation ICP-MS study). Chem Geol 117:291–312

Broska I, Petrik I, Williams CT (2000) Coexisting monazite and allanite in peraluminous granitoids of the Tribec Mountains, western Carpathians. Am Mineral 85:22–32

Casillas R, Nagy G, Panto G, Brandle J, Forizs I (1995) Occurrence of Th, U, Y, Zr and REE bearing minerals in late Variscan granitic rocks from the Sierra Guadarrama (Spain). Eur J Mineral 7:989–1006

Cheburkin A, Frei R, Shotyk W (1997) An energy-dispersive miniprobe multielement analyzer (EMMA) for direct analysis of trace elements and chemical age dating of single mineral grains. Chem Geol 135:75–87

Davidson C, Rosenberg C, Schmid SM (1996) Synmagmatic folding of the base of the Bergell pluton, central Alps. Tectonophysics 265:213–238

Fitzsimonis ICW (1996) Metapelitic migmatites from Battstrand Bluffs, East Antarctica – metamorphism, melting and exhumation of the mid crust. J Petrol 37:395–414

Fourcade S, Martin H, de Bremond D, Ars J (1992) Chemical exchange in migmatites during cooling. Lithos 28:43–53

Green TH (1994) Experimental studies of trace-element partitioning applicable to igneous petrogenesis – Sedona 16 years later. Chem Geol 117(1–4):1–36

Hanson GH (1978) The application of trace elements to the petrogenesis of igneous rock of granitic composition. Earth Planet Sci Lett 38:26–43

Hanson RB, Barton MD (1989) Thermal development of low-pressure metamorphic belts: results from two-dimensional numerical models. J Geophys Res 94(B8):10363–377

Holness MB, Clemens J (1999) Partial melting of the Appin Quartzite driven by fracture-controlled H_2O infiltration in the aureole of the Ballachulish Igneous Complex, Scottish Highlands. Contrib Mineral Petrol 136:154–168

Holtz F, Scaillet B, Behrens H, Schulze F, Pichavant M (1996) Water contents of felsic melts: application to the rheological properties of granitic magmas. Trans R Soc Edinb Earth Sci 87:57–64

Icenhower J, London, D (1996) Experimental partitioning of Rb, Cs, Sr and Ba between alkali-feldspar and peraluminous melt. Am Mineral 81:719–734

Jin Z, Green HW, Zhou Y (1994) Melt topology in partially molten mantle peridotite during ductile deformation. Nature 372:164–167

Johannes W, Holtz F (1996) Petrogenesis and experimental petrology of granitic rocks. Springer, Berlin Heidelberg New York

Johannes W, Koepke J, Behrens H (1994) Partial melting reactions of plagioclase and plagioclase bearing systems. In: Parsons I (ed) Feldspars and their reactions. NATO Advanced Study Institutes series. Series C, Mathematical and physical sciences, vol 421. Reidel, Dordrecht, pp 161–194

Johannes W, Holtz F, Muller P (1995) REE distribution in some layered migmatites constraints on their petrogenesis. Lithos 35:135–152

Jung S, Mezger K, Masberg P, Hoffer P, Hoernes S (1998) Petrology of an intrusion related high grade migmatite: implications for partial melting of metasedimentary rocks and leucosome forming processes. J Metamorph Geol 16:425–445

Langmuir CH, Klein EM, Plank T (1992) Petrological systematics of mid ocean ridge basalts: constraints on melt generation beneath ocean ridges. Geophys Monogr 71:183–280

Mahood G, Hildreth W (1983) Large partition coefficients for trace elements in high silica rhyolites. Geochim Cosmochim Acta 47:11–30

Misch P (1968) Plagioclase composition and non anatectic origin of migmatitic gneisses in northern Cascade Mountains of Washington State. Contrib Mineral Petrol 17:1–70

Montel JM (1993) A model for monazite/melt equilibrium and application to the generation of granitic magmas. Chem Geol 110:127–146

Nabelek PI (1999) Trace element distribution among rock forming minerals in Black Hills migmatites South Dakota: a case for solid state equilibrium. Am Mineral 84:1256–1269

Nabelek PI, Glascock MD (1995) REE-depleted leucogranites. Black Hills South Dakota: a consequence of disequilibrium melting of monazite bearing schists. J Petrol 36:1055–1071

Nash WP, Crecraft HR (1985) Partition coefficients for trace elements in silicic magmas. Geochim Cosmochim Acta 49:2309–2322

Obata M, Yoshimura Y, Nagakawa K, Odawara S, Osanai Y (1994) Crustal anatexis and melt migration in the Higo metamorphic terrane, west Central Kyushu, Kumamoto, Japan. Lithos 32:135–147

Paterson MS (1995) A theory for granular flow accommodated by material transfer via an intergranular fluid. Tectonophysics 245:135–151

Paterson MS (2001) A granular flow theory for the deformation of partially molten rock. Tectonophysics 335:51–61

Rosenberg CL, Berger A (2001) Syntectonic melt pathways in granitic gneisses, and melt-induced transition in deformation mechanisms. Phys Chem Earth 26(4–5):287–293

Rosenberg CL, Handy M (2001) Mechanisms and orientation of melt segregation paths during pure shearing of a partially molten rock analog (norcamphor-benzamide). J Struct Geol 23:1917–1932

Rosenberg CL, Riller U (2000) Partial melt topology in statically and dynamically recrystallized granite. Geology 28:7–10

Rosenberg CL, Berger A, Schmid SM (1995) Observation on the floor of a granitoid pluton; inferences on the driving force of final emplacement. Geology 23:443–446

Sawyer EW (1991) Disequilibrium melting and the rate of melt-residuum separation during migmatization of mafic rocks from the Greenville Front Quebec. J Petrol 32:701–738

Sawyer EW (1998) Formation and evolution of granite magmas during crustal reworking: the significance of diatexites. J Petrol 39:1147–1167

Sawyer EW (1999) Criteria for the recognition of partial melting. Phys Chem Earth 24:269–279

Sawyer EW (2001) Melt segregation in the continental crust: distribution and movement of melt in anatectic rocks. J Metamorph Geol 19:291–309

Sawyer EW, Barnes SJ (1988) Temporal and compositional differences between subsolidus and anatectic migmatite leucosomes from the Quetico metasedimentary belt, Canada. J Metamorph Geol 6:437–450

Singh J, Johannes W (1996) Dehydration melting of tonalites. Part 1: beginning of melting. Contrib Mineral Petrol 125:16–25

Trommsdorff V, Conolly J (1996) The ultramafic contact aureole about the Bregaglia (Bergell) tonalite: isograds and a thermal model. Schweiz Mineral Petrogr Mitt 76:537–547

Tullis J, Yund R, Farver J (1996) Deformation-enhanced fluid distribution in feldspar aggregates and implications for ductile shear zones. Geology 24:63–66

Watson EB, Harrison TM (1983) Zircon saturation revisited: temperature and composition effects in variety of crustal magma types. Earth Planet Sci Lett 64:295–304

Watt GR, Burns IM, Graham GA (1996) Chemical characteristics of migmatites: accessory phase distribution and evidence for fast melt segregation. Contrib Mineral Petrol 125:100–111

Whitney DL, Irving AJ (1994) Origin of K-poor leucosomes in a metasedimentary migmatite complex by ultrametamorphism, syn-metamorphic magmatism and subsolidus processes. Lithos 32:173–192

Yund RA (1986) Interdiffusion of NaSi–CaAl in peristerite. Phys Chem Mineral 13:11–16

Yund RA, Tullis J (1991) Compositional changes of minerals associated with dynamic recrystallization. Contrib Mineral Petrol 108:346–355